Journal of Power Sources 188 (2009) 148–155

Contents lists available at ScienceDirect

Journal of Power Sources

journal homepage: www.elsevier.com/locate/jpowsour

Comparative study of perovskites as cathode contact materials between an $La_{0.8}Sr_{0.2}FeO_3$ cathode and a Crofer22APU interconnect in solid oxide fuel cells

X. Montero[a,b,*], F. Tietz[b], D. Stöver[c], M. Cassir[c], I. Villarreal[a]

[a] Ikerlan-Energia, Parque Tecnologico de Alava, Juan de La Cierva 1, 01501 Miñano, Spain
[b] Forschungszentrum Jülich GmbH, Institute for Materials and Processes in Energy Systems, 52428 Jülich, Germany
[c] LECA UMR7575 CNRS-ENSCP-Paris6, 11 rue Pierre et Marie Curie, 75231 Paris Cedex 05, France

ARTICLE INFO

Article history:
Received 27 August 2008
Received in revised form 30 October 2008
Accepted 22 November 2008
Available online 28 November 2008

Keywords:
SOFC
Interconnect
Cathode contact material
ASR

ABSTRACT

Perovskites of different compositions were tested as cathode contact material between an $La_{0.8}Sr_{0.2}FeO_3$ cathode and a Crofer22APU interconnect by resistance measurements at 800 °C. The materials tested were $LaNi_{0.6}Fe_{0.4}O_3$ and $La_{0.8}Sr_{0.2}FeO_3$ which are also used as cathodes; $La_{0.8}Sr_{0.2}Mn_{0.5}Co_{0.5}O_3$ and $La_{0.8}Sr_{0.2}Mn_{0.1}Co_{0.3}Fe_{0.6}O_3$, selected for comparing perovskites with different Mn contents; and $La_{0.8}Sr_{0.2}Co_{0.75}Fe_{0.25}O_3$ and $La_{0.8}Sr_{0.2}Co_{0.75}Cu_{0.25}O_3$ for comparing perovskites with high Co content and two possible partial substitutions of the Co. The initial area-specific contact resistance (ASR) was found to depend on the electrical conductivity of the measured perovskites. Time evolution of the ASR depended on the interactions between the contact material and the interconnect, showing the highest degradation rates for $LaNi_{0.6}Fe_{0.4}O_3$ and $La_{0.8}Sr_{0.2}FeO_3$. Chromium from the interconnect reacted with the Sr-containing perovskites forming $SrCrO_4$. With the contact material without strontium chromium-containing perovskites were formed. A reduced interfacial reaction was achieved by application of a $MnCo_{1.9}Fe_{0.1}O_4$ spinel protection layer on Crofer22APU in terms resulting in low and stable ASR.

1. Introduction

Solid oxide fuel cells (SOFC) produce electricity and heat by electrochemically combining fuel and air across an ionic conducting electrolyte membrane. Such energy production is highly interesting because public awareness has been raised for limitations of greenhouse gas emissions, increase in efficiency of energy conversion systems and decentralised energy conversion systems [1–3]. However, a single SOFC only produces less than one volt. Therefore, to achieve useful voltages, a number of cells are usually electrically connected in series in a "stack" via interconnects which also separate the fuel at the anode side of one cell from the air at the cathode side of the adjacent cell. The interconnect must be electrically conducting, gastight, chemically stable towards the adjacent electrodes, cost-effective and have a matching thermal expansion coefficient (TEC) to those of the other cell components [4–6].

One of the challenges in SOFC development is the power loss within the stack due to high contact resistances between the interconnects and the electrodes [6]. The tubular SOFC design, which Ikerlan is trying to develop for generating electricity and heat in domestic use, should operate in the range between 600 and 800 °C and the supporting tube as well as the cathode side current collector are metallic components [7,8]. It has been demonstrated that the ferritic steels forming $MnCr_2O_4/Cr_2O_3$ oxide under oxidising SOFC operating conditions, substantially reduce the Cr evaporation [9]. Among the steels forming such layers Crofer22APU steel has received considerable attention, because it shows a low oxidation rate, well adherent and highly conductive oxide scales [9]. However, the Cr evaporation is still elevated and could affect the catalytic activity of the cathode leading to cell degradation [10].

Therefore, interaction of the metallic interconnects with the cathode and the resulting time-dependent resistance of the material combinations is highly important. To achieve good electrical contact between the interconnects and the cathodes, additional materials are used in stack assembly. Such cathode contact materials (CCM) have no direct role in the electrochemical reactions, but they can provide a homogeneous contact over the whole area of the fuel cell and minimise the ohmic losses within the stack. A chemical interaction between the CCM and a cathode or the interconnect should not occur, but cannot be avoided in most cases due to the reaction of the CCM with the chromia scale formed on the interconnect. Accordingly, there is a need for suitable CCM to minimise the interfacial electrical resistance and maximise the power output of SOFC stacks.

The attempted realization of a cost-effective system excludes the use of expensive noble metals as the CCM. Even if Ag or Ag-containing Ni alloys have a lower cost than noble metals, their high

* Corresponding author at: Ikerlan-Energia, Parque Tecnologico de Alava, Juan de La Cierva 1, 01501 Miñano, Spain. Tel.: +34 945297032; fax: +34 945296926.
E-mail address: xmontero@ikerlan.es (X. Montero).

0378-7753/$ – see front matter © 2008 Elsevier B.V. All rights reserved.
doi:10.1016/j.jpowsour.2008.11.083

Table 1
Composition of the steel in wt%.

	Fe	Cr	Mn	Ti	Si	Al	Mo	Others
Crofer22APU	76.45	22.78	0.4	0.07	0.02	0.006	–	La 0.086

volatility and rapid thermal etching in hot air may limit their use in SOFCs operating at relative high temperatures [11,12]. Therefore, the use of perovskites as the CCM seems to be more adequate. Several research groups have been making efforts to develop different compositions of CCM.

Perovskites such as La(Co,Cr,Mn,Ni,Fe)O_3 have been tested but their low conductivity and their poor sinterability complicate their use [13–15]. The introduction of alkali-earth elements such as Ca, Ba or Sr increases the sintering activity and the conductivity of such perovskites [6]; however, an excess of these elements causes rapid cell deterioration through the formation of low mechanical strength phases (referred in the text as brittle phases) such as $SrCrO_4$, $CaCrO_4$ or $BaCrO_4$ by the reaction with the Cr released from the interconnect [16–18]. Therefore, perovskites with small additions of Sr such as $La_{0.8}Sr_{0.2}$(Co,Cu,Fe)O_3, $La_{0.8}Sr_{0.2}$(Co,Mn,Fe)O_3, $La_{0.8}Sr_{0.2}$(Mn,Cu,Fe)O_3 have been recently studied by several authors, showing an adequate sintering activity, electrical conductivity and low brittle phase formation [15,19,20]. These studies have concluded that (i) high amounts of cobalt increase the conductivity and the TEC of the CCM [21], (ii) high amounts of Mn enhance the formation of Mn–Cr spinels by reaction with the Cr released from the interconnect [22] and that they (iii) exhibit a less pronounced tendency to release strontium from the crystalline lattice than cobaltite-based perovskites [23] and that (iv) little amounts of Cu are necessary for achieving high densification in perovskites [24,25].

In the present study, several perovskites were investigated as potential contact materials. Results of the investigation of their electrical performance and chemical stability in combination with Crofer22APU as interconnect material are presented and discussed.

2. Experimental

The influence of several cathode contact materials was studied at 800 °C in air on Crofer22APU (ThyssenKrupp VDM, Werdohl, Germany). The composition of the steel, given by the supplier, is listed in Table 1. Even if the envisaged SOFC is tubular-shaped, all the tests were carried out with flat samples for an easier experimental mounting and characterisation.

Area-specific resistance (ASR) measurements were carried out as shown in Fig. 1. After cutting in 10 mm × 10 mm × 1 mm pieces, polishing and cleaning, the alloy was coated by screen-printing with the different CCM. The pastes were produced by milling several times a mixture of powder and a solution based on therpineol and ethylcellulose through a three roll milling machine. The paste was passed through a mask of a specific wire diameter, which gave the thickness of the applied layer in the wet state. After deposition of the layers, the samples were dried in a furnace at 60–70 °C. A mask of 180 μm was used which usually gave a cathode contact material layer of around 60 μm after sintering. The $La_{0.8}Sr_{0.2}Co_{0.75}Cu_{0.25}O_3$ (LSCCu), $La_{0.8}Sr_{0.2}Co_{0.75}Fe_{0.25}O_3$ (LSCF) and $LaNi_{0.6}Fe_{0.4}O_3$ (LNF) powders were produced by the Pechini method [18]. The $La_{0.8}Sr_{0.2}FeO_3$ (LSF) powder was produced by spray pyrolysis. The $La_{0.8}Sr_{0.2}Co_{0.5}Mn_{0.5}O_3$ (LSCM) and $La_{0.8}Sr_{0.2}Co_{0.3}Mn_{0.1}Fe_{0.6}O_3$ (LSCMF) powders were supplied by H.C. Starck (Goslar, Germany). X-ray diffraction of these powders after calcinations at 900 °C were carried out by a Siemens D5000 diffractometer and Cu $K_{\alpha 1}$ radiation (λ = 1.54 Å). The LSF cathode pellets were manufactured by the Coat-Mix® method [19] and sintered at 1100 °C. The assembling of the coated steels with the LSF cathode was carried out by heat treatment at 850 °C for 10 h. The ASR measurement begin after the assembling step, when the temperature was stabilised at 800 °C. A 0.5 kg cm^{-2} weight was uniformly loaded onto the samples in order to achieve a better mechanical contact during measurement. A current density of 0.3 A cm^{-2} was applied during the resistance measurement using a 4 point DC setup for up to 300 h.

The microstructure and cross-section of the samples after ASR measurement were characterised by scanning electron microscopy (SEM, Zeiss Ultra55), combined with energy dispersive X-ray spectroscopy (EDX, INCA, Oxford Instruments and SDD X-FLASH 4010, BRUKER). After the cross-section analysis, the samples were cut out of the epoxy resin in which they were embedded. LSF of the samples was removed by polishing, so that the X-ray diffraction (XRD) of the CCM coated steel after ASR measurement could be done. The XRD were carried out by a Siemens D5000 diffractometer and Co $K_{\alpha 1}$ radiation (λ = 1.78892 Å).

ASR tests were also performed up to 1000 h with Crofer22APU coated with a $MnCo_{1.9}Fe_{0.1}O_4$ (MCF) spinel layer. This MCF is intended to serve as a barrier to chromium cation diffusion, so that it can mitigate or even prevent chromium migration from the steel to the cathode. The spinel layer was applied by screen-printing onto polished and cleaned Crofer22APU samples. A mask of 60 μm was used which usually gave a protective $MnCo_{1.9}Fe_{0.1}O_4$ layer of around 10 μm after sintering. A thermal treatment under a reductive atmosphere followed by a reoxidation step, referred here as reactive sintering, was applied to the coated samples to obtain a higher densification of the spinel layer. Details of the preparation of the spinel protection layer can be found in [26]. The LSCCu LSCMF,

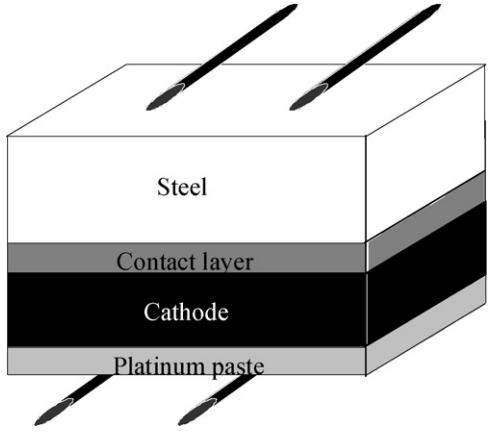

Fig. 1. Sample setup for ASR measurements for steel–cathode contact resistances.

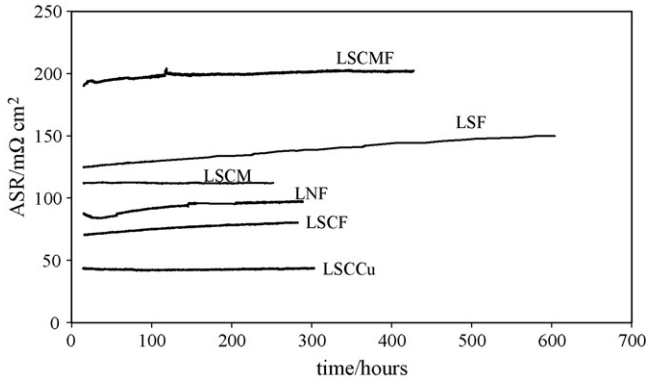

Fig. 2. ASR for Crofer22APU/CCM/LSF interfaces as a function of time with different cathode contact materials.

Table 2
Initial ASR, bulk conductivity increase of ASR fitted to a lineal function and TEC of different CCM at 800 °C in air.

	LSCCu	LSCF	LNF	LSCM	LSF	LSCMF
ASR_0 ($m\Omega\,cm^2$)	43.4	70.5	86.4	112	124.9	191.3
σ ($S\,cm^{-1}$)	1074 [25]	724 [21]	463 [39]	175 [21]	110 [21]	100 [21]
ASR increase ($m\Omega\,cm^2\,h^{-1}$)	0.003	0.036	0.048	−0.002	0.045	0.019
TEC ($K^{-1} \times 10^{-6}$)	17.7	19	11.8	15.6	12.3	16

LSCF and LSCM cathode contact layers were tested in combination with MCF. The microstructure and cross-section of the samples after ASR measurement were characterised by SEM combined with EDX.

3. Results and discussion

3.1. ASR measurements

Fig. 2 shows the evolution of the ASR of different tested perovskites as a function of time. It should be noted that the ASR of the LSF pellet is ≈27 $m\Omega\,cm^2$ at 800 °C. As expected, the initial resistance is influenced by the electrical conductivity of the perovskites (see Table 2). However, no direct correlation between the bulk conductivity of the tested CCM and the ASR measurements could be done because in the ASR measurements should be taken into account apart of the bulk material conductivity, interactions of materials due to assembling processes as well as interfacial contact effects which usually are detrimental for contact resistances as will be follow explained.

The slopes of the ASR were different depending on the perovskite. Except for LSCCu and LSCM, the perovskites tested exhibited an increasing ASR over the measured time. For LSCMF, LNF and LSCF, initially the ASR increased quickly and then increased more slowly. For LSF and LSCF, the ASR increased steadily over the measured time. The difference in the ASR slopes is likely due to interactions between the growing oxide scale and the contact materials. A summary of the slopes is shown in Table 2. These values were obtained assuming a linear evolution of the measured ASR over time for the different samples. The highest increase was calculated for LNF and LSF, both materials regarded as Cr-tolerant cathode materials [27–29]. LSCF showed the next highest increasing rate followed by LSCMF.

3.2. Microstructural investigations

As mentioned before, interactions between interconnect and contact material can potentially have a significant effect on the magnitude and stability of the contact resistance. Therefore, the chemical compatibility between Crofer22APU and the perovskite-based contact materials was investigated.

The XRD results of the CCM powders heat-treated at 900 °C in air for 6 h, presented in Fig. 3, reveal that the main phase is a perovskite

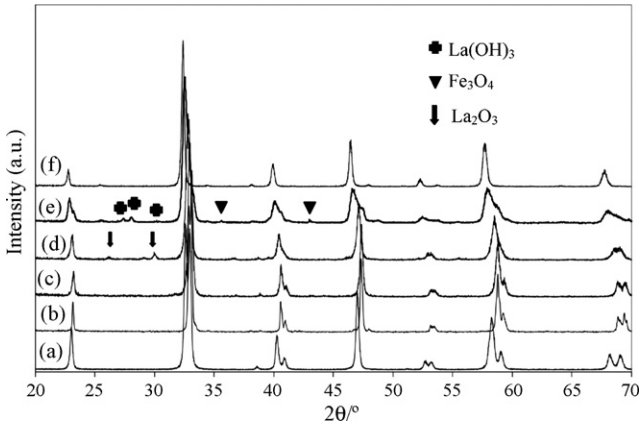

Fig. 3. XRD patterns at room temperature of CCM powders after calcination at 900 °C for: (a) LNF, (b) LSCCu, (c) LSCF, (d) LSCM, (e) LSCMF and (f) LSF.

in all cases. However, a small amount of impurities can be detected for the LSCM and LSCMF. La_2O_3 has been detected in the case of the LSCM, The LSCMF shows $La(OH)_3$ probably due to hydrolysis of La_2O_3 (usually happens after long storage periods in ambient air) and Fe_3O_4 as impurities.

The cross-sections of manganese-containing contact materials analysed after ASR measurement at 800 °C are shown in Fig. 4. The particle size of the LSCM layer was finer than for LSCMF. LSCMF showed the formation of $SrCrO_4$ (also confirmed by XRD, see Fig. 8) in large agglomerations all around the contact material, but no Cr was detected at the cathode. $SrCrO_4$ formation was also detected in LSCM, but mainly concentrated close to the interface with the Crofer22APU. It is important to note that the interface between both cathode contact materials and Crofer22APU shows large areas without contact, which could affect strongly in the measured resistance. In this case, large amounts of Co were detected all around the contact material, which form $(Mn,Co,Cr)_3O_4$ spinels in the oxide scale formed on the Crofer22APU. Due to small size of the novel phases, by EDX analysis the chemical composition cannot be identified precisely, because the interaction volume between the electrons and the material to be characterized is larger than the changed regions. As in the previous case, no Cr was detected in the LSF cathode.

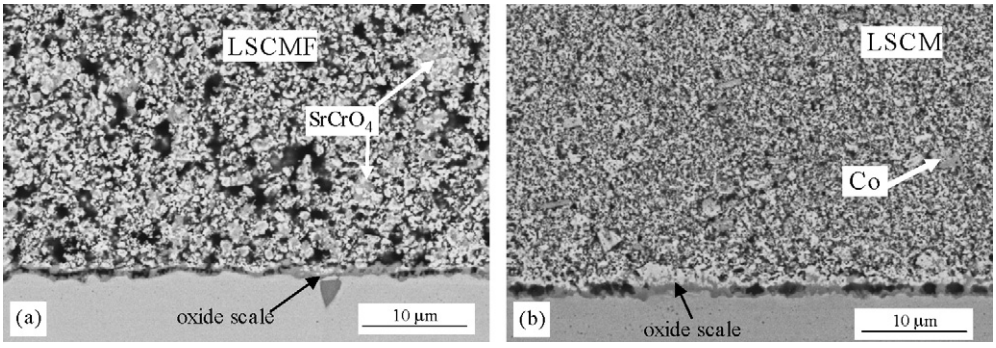

Fig. 4. SEM cross-section of the Crofer22APU/CCM/LSF after ASR measurement at 800 °C for LSCMF (a) and LSCM (b).

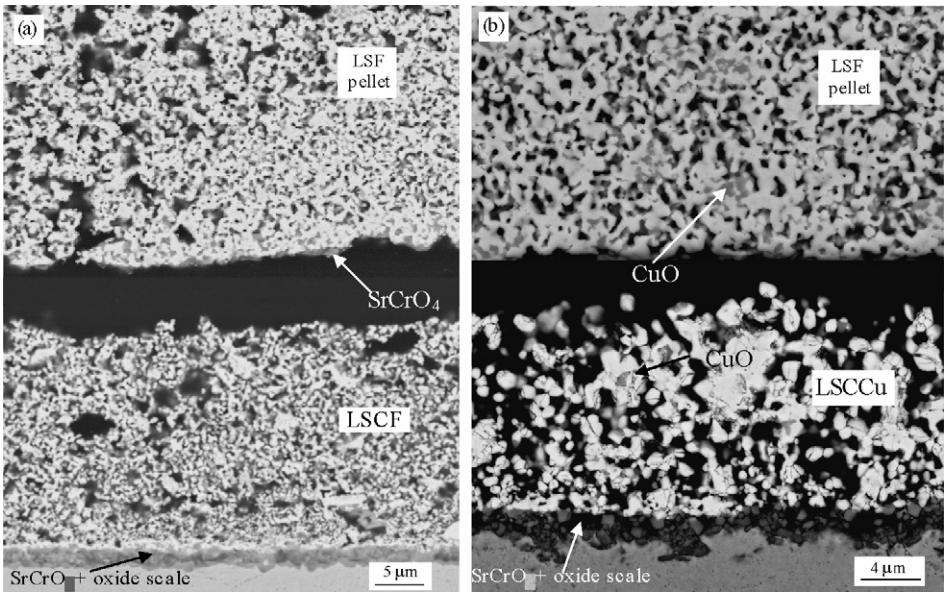

Fig. 5. SEM cross-section of Crofer22APU/CCM/LSF after ASR measurement in air at 800 °C for LSCF (a) and LSCCu (b).

In accordance with literature [19,20], perovskites with high Mn content, facilitate the formation of Mn-containing spinels, as observed for LSCM. Moreover, the conductivity of the Mn-containing spinels increase with Co content. Therefore, the formation of these spinels could be related to the low degradation observed for the ASR of this contact material. The XRD analysis of the sample after ASR measurement (see Fig. 8) indeed showed Mn-containing spinels, but this could be more related to the oxide scale formation on the Crofer22APU.

The conductivity of the contact materials and the formation of the Co-containing spinels at the oxide scale increased with increasing Co content. For a better understanding of the influence of Co in the CCM, the comparison of LSCF and LSCCu as CCM with higher Co amounts, is presented in Fig. 5.

The contact layers were well bonded to the metallic substrate but the cathode was not attached after the measurement (Fig. 5). This observation could be related to the high TEC observed with the high Co-containing CCM (see Table 2) [21]. When the LSCF contact material was used (Fig. 5a), an oxide scale with many different compositions was formed as result of the interaction between the Crofer22APU and the applied contact material layer. Chromia was formed on top of the Crofer22APU. Above this chromia layer a continuous $SrCrO_4$ layer was found and finally, between $SrCrO_4$ and the LSCF contact material, a white coloured thin and uniform $(La,Sr)(Cr,Mn)O_3$ layer was formed. $SrCrO_4$ grains were also formed within the contact layer and the LSF cathode material. The increase observed in the ASR measurement for the LSCF-coated Crofer22APU sample is attributed to the formation of Cr-containing perovskite and $SrCrO_4$.

When LSCCu was used (Fig. 5b), a multi-compositional oxide scale is also formed. On top of the chromia scale, $SrCrO_4$ was formed as in the previous case; however, between this layer and the LSCCu layer, a $(Mn,Co,Cu)_3O_4$ spinel was formed as result of the reaction between the Mn diffusing from the Crofer22APU and the Co and

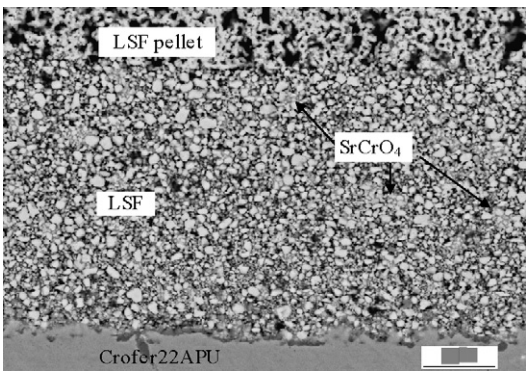

Fig. 6. SEM cross-section of Crofer22APU/LSF/LSF after ASR measurement in air at 800 °C.

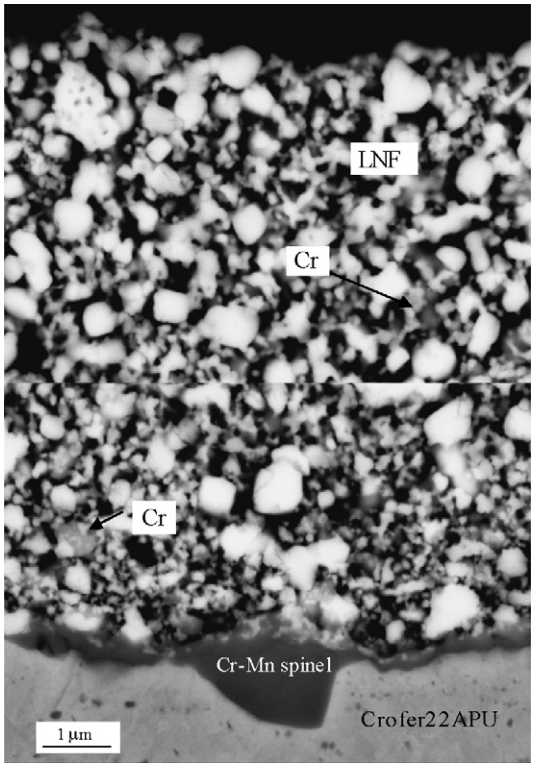

Fig. 7. SEM cross-section of Crofer22APU/LNF/LSF after ASR measurement in air at 800 °C.

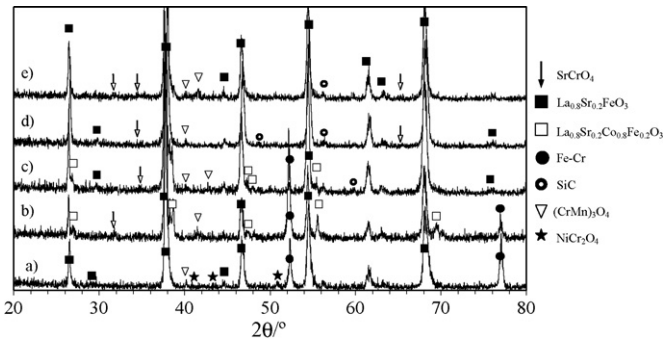

Fig. 8. XRD patterns of Crofer22APU/CCM/LSF after ASR measurement in air at 800 °C for: (a) LSF, (b) LSCCu, (c) LSCF, (d) LSCM and (e) LSCMF.

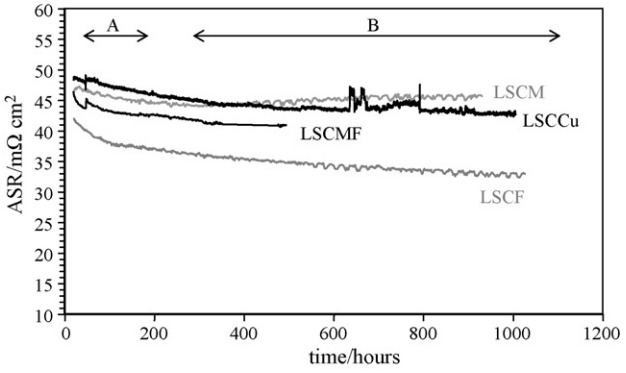

Fig. 9. ASR measurement in air at 800 °C of Crofer22APU/MCF/CCM/LSF, with LSCCu, LSCM, LSCF and LSCMF as CCM.

Table 3
Initial ASR, slopes of ASR for the different intervals and chromia thickness after ASR measurement for the Crofer22APU coated with MCF and different CCM.

	LSCCu	LSCM	LSCMF	LSCF
ASR_0 (mΩ cm^2)	48.3	46.6	46.3	41.7
Interval A ($\times 10^3$ mΩ cm^2 h^{-1})	−13.9	−10.5	−18.9	−41.9
Interval B ($\times 10^3$ mΩ cm^2 h^{-1})	−1.9	2.6	−6.4	−5.3
Intersection between interval A and B (h)	300	300	150	120
Chromia thickness	0.26	0.33	0.44	0.4

Cu present in the CCM. The Cu content in the LSCCu was not stable enough and precipitated in the CCM as CuO particles which were also found in the LSF cathode as result of evaporation [30,31]. However, the presence of CuO was not detected in the XRD analysis of this sample (see Fig. 8). No Cr was found in the LSF pellet. As observed for LSCM, the formation of a high conductivity spinel seems to be again the possible explanation for the low degradation of ASR observed for the LSCCu sample [32].

When LSF was used as a cathode contact material (Fig. 6), the sintering activity seemed to be very low. However, a good adherence was obtained between the Crofer22APU and the cathode pellet. Large amounts of $SrCrO_4$ were detected within the LSF contact layer as indicated in the figure.

Fig. 7 shows the SEM cross-section of the LNF-coated sample after ASR measurement. As observed in the previous case, the sintering activity also seems to be low. Apparently, high Fe content seems to be disadvantageous for the sintering behaviour of the perovskites. In this case, the Cr-containing dark coloured perovskites were detected within the cathode contact material. These perovskites are rich in Mn close to the Crofer22APU. The oxide scale formed on the Crofer22APU contains Ni–Cr oxides and Cr–Mn spinels (verified by XRD). Apparently small amounts of NiO were released from the LNF perovskite [13], which reacted with the Cr from the Crofer22APU.

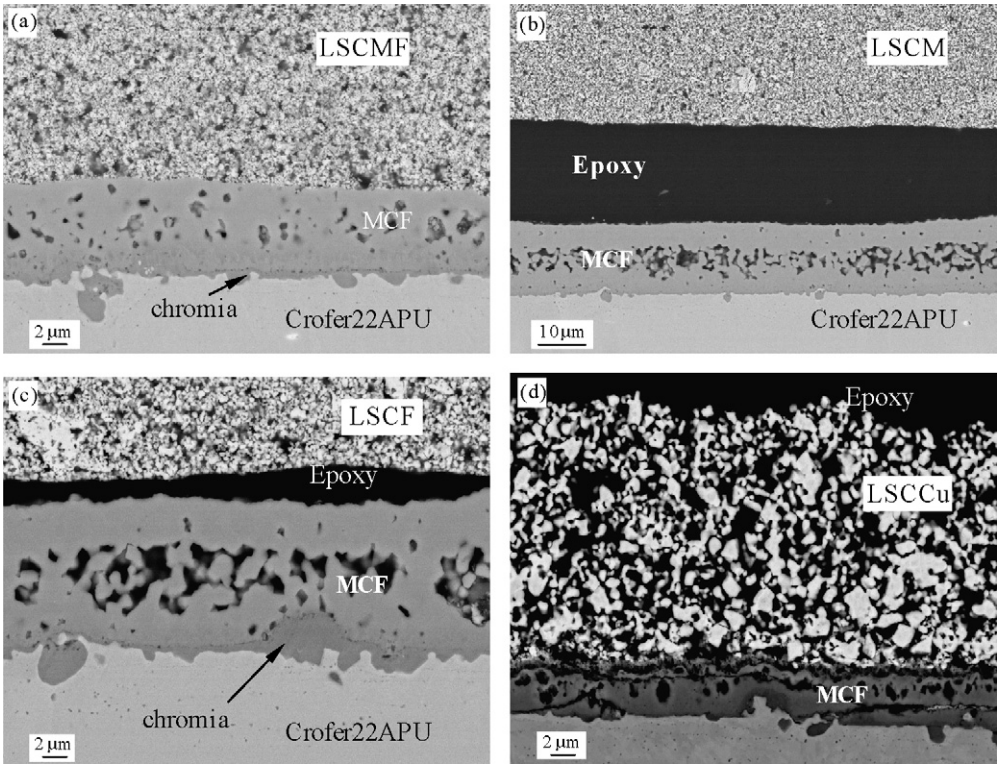

Fig. 10. SEM cross-section of Crofer22APU coated with MCF protective layer and LSCMF (a), LSCM (b), LSCF (c) or LSCCu (d) after ASR measurement in air up to 1000 h.

The X-ray diffraction study (Fig. 8) seems to be in accordance with the previous observations of the interaction between the perovskites and the Crofer22APU. However, it should be pointed out that only limited information can be obtained from these patterns. The complexity of the materials system shows in some cases shift of reflections due to different compositions in one crystalline phase. For the preparation of the samples, the LSF cathode pellet was scraped off carefully by using a SiC abrasive paper, which was detected in the patterns.

3.3. Crofer22APU coated with an MCF protection layer

The ASR of Crofer22APU coated with an MCF spinel was tested for up to 1000 h at 800 °C by using LSCCu, LSCM, LSCF and LSCMF as cathode contact materials. Contrary to the cases where no MCF was applied (compare Figs. 2 and 9), the resistance values were found in the same range, between 30 and 50 mΩ cm^2, regardless of the applied cathode contact material.

As calculated in Table 2, the evolution of ASR for this set of samples can be divided into two time-dependent intervals. An initial period, interval A, with a duration of between 120 and 300 h, showing a fast resistance decrease and a long-term exposure period, interval B, showing an slow increasing resistance for the LSCM and a decreasing one for the other three CCM. The evolution of the ASR measurements might have been dependant on several factors, including scale growth beneath the protection layer (tending to increase ASR) and improvement in the electrical contact at the MCF/CCM interface (which might tend to decrease the ASR) [26,33].

SEM analysis on the cross-sections of the tested samples (Fig. 10) indicated that the spinel coatings were well bonded to the Crofer22APU and free of spallation but with remaining porosity. The chromia layer formed between the Crofer22APU and the applied MCF coating had a thickness of between 0.3 and 0.4 μm (measured directly from the SEM images and listed in Table 3), which is very similar to the chromia growing on Crofer22APU in air at 800 °C without any coating [34]. As reported previously [26] and observed in Fig. 11, a reaction zone was formed in the MCF coating applied beneath the chromia scale containing Mn–Co–Cr spinels. The reaction zone seems to be formed during the reduction step of the reactive sintering by the reaction between the Mn–Cr spinel formed on the Crofer22APU and the reduced Co from the MCF spinel. The MCF spinel was free of Cr outside this reaction zone.

The LSCMF contact material remained unchanged apart from the Mn enrichment observed in the area beneath the MCF coating. Good

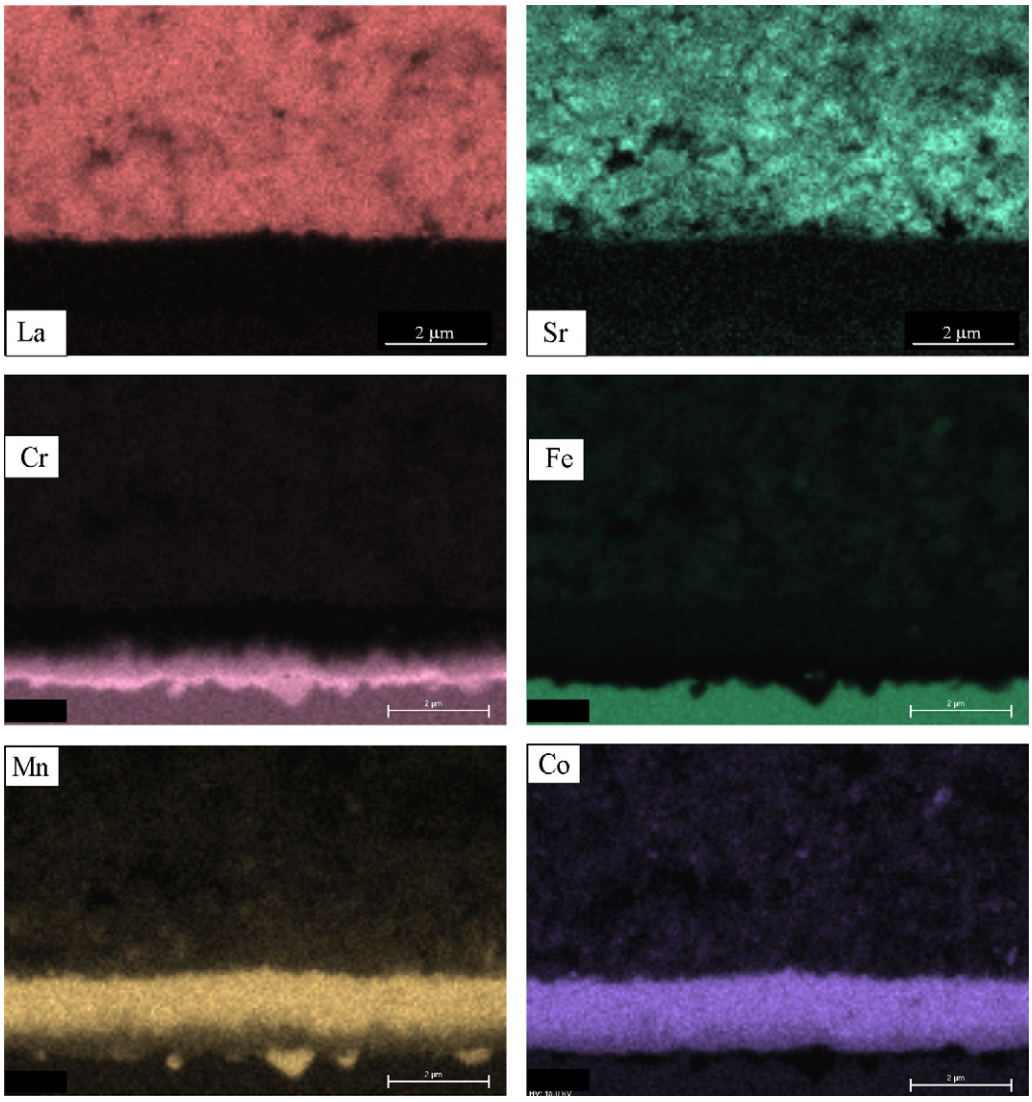

Fig. 11. EDX mapping of the cross-section of Crofer22APU coated with MCF protective layer and LSCMF contact materials after ASR measurement in air at 800 °C.

adherence was observed between both layers. No Cr was detected in the contact material as confirmed in the detailed EDX mapping of the interface (Fig. 11) neither in the LSF pellet.

White coloured 2 μm La-rich agglomerations were observed in the LSCM contact layer, probably due to an incomplete reaction or excess of La during the Pechini synthesis of the powder. Loss of adherence was observed between the protection and contact layer during cooling down to room temperature.

White and grey coloured La and Co-rich agglomerations, respectively, were observed in the LSCF contact layer, probably for the same reasons as the previous case. Mn is detected in the contact material close to the MCF coating, presumably from the protective spinel layer. No Cr has been detected in the LSCF or either the LSF pellet. In this case, loss of adherence is also observed between the protection and contact layer during cooling down to room temperature.

When LSCCu is used as a contact material, the MCF protective layer is enriched in Cu due to the diffusion and evaporation of the Cu species. This enrichment contributes to a higher densification of the MCF coating showing some cracks as consequence of this densification. Similar to the observations of Fig. 5b, binary Cu oxide was detected in the LSCCu and in the LSF cathode as a decomposition product with high vapour pressure. The LSCCu region close to the MCF layer was enriched in Mn.

The initial resistance is mainly attributed to the spinel protective layer. The presence of the MCF overrides the interaction between the Crofer22APU and the different CCMs during the assembling of the samples at 850 °C, decreasing the formation of low conductivity perovskites reported for the previous cases and increases the surface contact, decreasing as a result the resistance in comparison to the cases where no MCF was applied. The small differences of ASR observed between the four cases analysed are mainly due to compositional changes in the MCF, due to the interactions of the MCF with the different contact materials. It has been reported in the literature that the conductivity of $Mn_{1-x}Co_{2-x}O_4$ or $(Mn,Co,Fe)_3O_4$ spinels decreased when their Mn content increases [35–37]; therefore, the initial resistance observed for the LSCM and LSCMF is very similar and higher than that observed for LSCF. However, the highest initial resistance was observed for LSCCu, in which high amounts of Cu were detected in the MCF beneath the cathode contact material. As reported in the literature [38], a decrease in electrical conductivity is also observed when Co is replaced with Cu in the $(Mn,Co)_3O_4$ spinel. Presumably, the impact of Cu on the decrease in conductivity of MCF is larger than that provoked by Mn.

The order of the initial resistances and the slopes calculated for interval A remain unchanged during the first 200 h of the ASR measurement. Therefore, the interaction between the spinel and the applied CCM is regarded as the main process during this interval. However, the improvement in the electrical contact between the spinel and the CCM led to the largest changes in resistance during the whole period of measurement.

The scale growth on Crofer22APU seems to affect the four measured contact layers in the same way. Therefore, the evolution of ASR in interval B is presumably related to the stability of the contact materials. The LSCCu and the LSCM contact materials showed the highest ASR value. The incorporation of Cu resulted in crack formation in the entire MCF protective layer and a continuous decrease of ASR, whereas for LSCM a small increase in ASR is observed. Apparently, the high Mn content in LSCM stabilised the perovskite and the main contribution to the time-dependence of the ASR is the interaction of MCF with the Cr released from the interconnect. A lower amount of Mn as in LSCMF seems to be a better compromise. Moreover, the low Co content of this perovskite could increase its stability in comparison with the LSCCu and LSCF as reported by Tietz et al. [23].

4. Conclusions

The initial value and the evolution of ASR are strongly influenced by the conductivity of the selected CCM. The initial value of the ASR without MCF coating is dependant of the conductivity of the perovskite and the interaction between the oxide formed on Crofer22APU and the different CCM during assembling. The evolution of the resistivity in dependant of the conductivity of the oxide scale formed on the steel, the reaction product between this oxide scale and the perovskite with whom is in contact and the conductivity of the perovskite (which may change in function of time due to the aforementioned reaction or stability of the perovskite). The use of a Sr-containing cathode contact material with Crofer22APU leads to the formation of $SrCrO_4$ and Cr-containing perovskites in short exposure times. When no Sr is present in the CCM, Cr-containing perovskites with low electrical conductivity are formed. The largest degradation in resistance was observed for LSF and LNF as contact materials.

When MCF is used as a protective layer, no Cr was found in the CCM and in the LSF cathode pellet. The presence of MCF overrides the interaction between oxides formed on Crofer22APU due to high temperature exposures and improves the contact between the interfaces, therefore, the ASR is mainly dependent on the conductivity of this spinel layer instead of the CCM applied. Thus, the choice of the CCM layer is dependent on its long-term stability. In the present case LSCMF is a suitable choice as CCM due to the higher stability and the adequate TEC match between the applied layers.

Acknowledgements

The authors gratefully acknowledge the provision of materials by the Real-SOFC programme. This work was supported financially by the strategic action GENEDIS (Etortek) of the Basque Country Government. The authors thank V. Bader (FZJ, IEF-1) for the technical assistance in the preparation of the powders, Dr. D. Sebold (FZJ, IEF-1) and S. Borensztajn (LISE, UMR7575) for the SEM/EDX analyses and Dr. O. Majerus from Laboratoire de Chimie de la Matière Condensée, at ENSCP for the XRD analyses. X.M. also thanks IEF-1 as host institution for continuous support of his Ph.D. work.

References

[1] D. Meadows, J. Randers, W. Behrens, Limits to Growth, Club of Rome, 1972.
[2] International Panel on Climate Change, Climate Change 2001: The Scientific Basis, Cambridge University Press, Cambridge, 2001, p. 850.
[3] L. S. Langston, Mechanical Engineering, Power & Energy 1 (2004), http://www.memagazine.org/supparch/pejun04/yearturb/yearturb.html.
[4] K. Hilpert, W.J. Quaddakers, L. Singheiser, Handbook of Fuel Cells—Fundamentals, Technology and Applications, Part 8, vol. 4, John Wiley & Sons, Ltd., Chichester, 2003, pp. 1037–1054.
[5] J.W. Fergus, Mater. Sci. Eng. A 397 (2005) 271.
[6] H.U. Anderson, F. Tietz, in: S.C. Singhal, K. Kendall (Eds.), High Temperature Solid Oxide Fuel Cells, Fundamentals, Design and Applications, Elsevier Science, The Netherlands, 2004 (Chapter 7).
[7] I. Villarreal, C. Jacobson, A. Leming, Y. Matus, S. Visco, L. De Jonghe, Electrochem. Solid State Lett. 6 (2003) 178.
[8] I. Antepara, I. Villarreal, L.M. Rodríguez-Martínez, N. Lecanda, U. Castro, A. Laresgoiti, J. Power Sources 151 (2005) 103.
[9] P. Huczkowski, N. Christiansen, V. Shemet, L. Niewolak, J. Piron-Abellan, L. Singheiser, W.J. Quadakkers, Fuel Cells 6 (2006) 93.
[10] M. Stanislowski, E. Wessel, K. Hilpert, T. Markus, L. Singheiser, J. Electrochem. Soc. 154 (2007) 295.
[11] B. Chalmers, R. King, R. Shuttleworth, Proc. R. Soc. A193 (1948) 465.
[12] E.D. Hondros, A.J.W. Moore, Acta Metall. 8 (1969) 647.
[13] R.N. Basu, F. Tietz, O. Teller, E. Wessel, H.P. Buchkremer, D. Stöver, J. Solid State Electrochem. 7 (2003) 416.
[14] Y. Larring, T. Norby, J. Electrochem. Soc. 147 (2000) 3251.
[15] E. Konysheva, J. Laatsch, E. Wessel, F. Tietz, N. Christiansen, L. Singheiser, K. Hilpert, Solid State Ionics 177 (2006) 923.
[16] N. Dekker, B. Rietveld, J. Laatsch, F. Tietz, in: M. Mogensen (Ed.), Proceedings of the 6th European Solid Oxide Fuel Cell Forum, 28 June–2 July 2004, Lucerne, 2004, p. 319.

[17] G.M. Christie, P.H. Middleton, B.C.H. Steele, in: H.I. Honolulu, S.C. Singhal, H. Iwahara (Eds.), Proceedings of the Third International Symposium on Solid Oxide Fuel Cells, 16–21 May 1993, Electrochemical Society, Pennington, NJ, 1993, p. 315.
[18] Y. Zhen, S.P. Jiang, J. Power Sources 180 (2008) 695.
[19] Z. Yang, G. Xia, P. Singh, J.W. Stevenson, J. Power Sources 155 (2006) 246.
[20] J. Pirón-Abellán, W.J. Quadakkers, Report Forschungszentrum Jülich, Jül 4170, 2005, ISBN 0944-2952.
[21] F. Tietz, I. Arul Raj, M. Zahid, D. Stöver, Solid State Ionics 177 (2007) 1753.
[22] W.J. Quadakkers, H. Greiner, M. Hänsel, A. Pattanaik, A.S. Khanna, W. Malléner, Solid State Ionics 91 (1996) 55.
[23] F. Tietz, A. Mai, D. Stöver, Solid State Ionics 179 (2008) 1509.
[24] S. Simner, M. Anderson, J. Bonnett, J. Stevenson, Solid State Ionics 175 (2004) 79.
[25] X. Montero, W. Fischer, F. Tietz, H.P. Buchkremer, A. Ringuedé, M. Cassir, A. Laresgoiti, I. Villarreal, Proceedings of the 8th European Solid Oxide Fuel Cell Forum, 30 June–4 July 2008, Lucerne, File No. A0918, 2008.
[26] X. Montero, F. Tietz, D. Sebold, H.P. Buchkremer, A. Ringuede, M. Cassir, A. Laresgoiti, I. Villarreal, J. Power Sources 184 (2008) 172.
[27] Y.D. Zhen, A.I.Y. Tok, S.P. Jiang, F.Y.C. Boey, J. Power Sources 170 (2007) 61.
[28] K. Kammer, L. Mikkelsen, J.B. Bilde-Sorensen, J. Solid State Electrochem. 10 (2006) 934.
[29] M. Krumpelt, T.A. Cruse, M.C. Hash, in: S.C. Singhal, J. Mizusaki (Eds.), Proceedings of the ninth International Symposia on Solid Oxide Fuel Cells (SOFC-IX), vol. 2005–07, The Electrochemical Society, Pennington, NJ, USA, 2005, p. 1578.
[30] N.H. Menzler, L.G.J. de Haart, D. Sebold, in: Proceedings of the 10th International Symposia on Solid Oxide Fuel Cells (SOFC-X), ECS Transactions 7 (1) (2007) 245.
[31] F. Tietz, D. Sebold, in: J.G. Heinrich, C. Aneziris (Eds.), Proceedings of the 10th International Conference and Exhibition of the European Ceramic Society (ECerS-10), 17–21 June, Berlin, 2007, p. 890.
[32] T. Kiefer, Ph.D. thesis, Report Forschungszentrum Jülich, Energy & Environment 3, 2008, ISBN: 978-3-89336-514-2.
[33] Z. Yang, G. Xia, C. Wang, Z. Nie, J. Templeton, J.W. Stevenson, P. Singh, J. Power Sources 183 (2008) 660.
[34] X. Montero, F. Tietz, D. Stöver, M. Cassir, I. Villarreal, Corros. Sci 51 (2009) 110.
[35] H. Ling, A. Petric, in: S.C. Singhal, J. Mizusaki (Eds.), Proceedings of the ninth International Symposia on Solid Oxide Fuel Cells (SOFC-IX), vol. 2005–07, The Electrochemical Society, Pennington, NJ, USA, 2005, p. 1866.
[36] Z. Yang, G. Xia, S.P. Simner, J.W. Stevenson, J. Electrochem. Soc. 152 (2005) 1896.
[37] T. Kiefer, M. Zahid, F. Tietz, D. Stöver, H.R. Zerfass, in: S. Linderoth, A. Smith, N. Bonanos, A. Hagen, L. Mikkelsen, K. Kammer, D. Lybye, P.V. Hendriksen, F.W. Poulsen, M. Mogensen, W.G. Wang (Eds.), Proceedings of the 26th Risø International Symposium on: Solid State Electrochemistry, Roskilde, Denmark, 2005, p. 261.
[38] A.V. Salker, S.M. Gurav, J. Mater. Sci. 35 (2000) 4713.
[39] R.N. Basu, F. Tietz, E. Wessel, H.P. Buchkremer, D. Stöver, Mater. Res. Bull. 39 (2004) 1335–1345.